The impact of Lyman α trapping on the formation of primordial objects

Latif, M. A.; Zaroubi, S.; Spaans, M.

Published in:
Monthly Notices of the Royal Astronomical Society

DOI:
10.1111/j.1365-2966.2010.17796.x

Publication date:
2011

Monthly Notices
of the
ROYAL ASTRONOMICAL SOCIETY

Mon. Not. R. Astron. Soc. **411,** 1659–1670 (2011) doi:10.1111/j.1365-2966.2010.17796.x

The impact of Lyman α trapping on the formation of primordial objects

M. A. Latif,[1⋆] S. Zaroubi[1,2] and M. Spaans[1]

[1] *Kapteyn Astronomical Institute, University of Groningen, PO Box 800, 9700 AV Groningen, the Netherlands*
[2] *Physics Department, Technion, Haifa 32000, Israel*

Accepted 2010 September 30. Received 2010 September 21; in original form 2010 July 2

ABSTRACT

Numerous cosmological simulations have been performed to study the formation of the first objects. We present the results of high-resolution 3D cosmological simulations of the formation of primordial objects using the adaptive mesh refinement code FLASH by including in an approximate manner the radiative transfer effects of Lyman α photons. We compare the results of a Lyman α trapping case inside gas clouds with atomic and molecular hydrogen cooling cases. The principal objective of this research is to follow the collapse of a zero metallicity halo with an effective equation of state (that accounts for the trapping) and to explore the fate of a halo in each of the three cases, specifically the impact of thermodynamics on the fragmentation of haloes. Our results show that in the case of Lyman α trapping, fragmentation is halted and a massive object is formed at the centre of a halo. The temperature of the gas remains well above 10^4 K and the halo is not able to fragment to stellar masses. In the atomic cooling case, gas collapses into one or two massive clumps in contrast to the Lyman α trapping case. For the molecular hydrogen cooling case, gas cools efficiently and fragments. The formation of massive primordial objects is thus strongly dependent on the thermodynamics of the gas. A salient feature of our results is that for the formation of massive objects, e.g. intermediate-mass black holes, feedback effects are not required to suppress H_2 cooling, as molecular hydrogen is collisionally dissociated at temperatures higher than 10^4 K as a consequence of Lyman α trapping.

Key words: methods: numerical – galaxies: formation – cosmology: theory – early Universe.

1 INTRODUCTION

The formation of primordial objects is not yet very well understood. A lot of progress has been made in analytical and numerical approaches but still further investigation is required. The formation of the first objects depends on the fragmentation process and its relation to thermodynamical properties of the gas (Ciardi & Ferrara 2005). In order to understand their formation, it is crucial to investigate the impact of thermodynamics on primordial haloes which define the mass scale of the first objects. It is generally believed that first stars are formed in minihaloes of $\sim 10^6\,M_\odot$ at redshift $z \sim 20$–30 while quasars are formed in massive haloes at $z \sim 10$ (Bromm 2004).

Numerical simulations performed to study the formation and fragmentation of primordial gas clouds (Tegmark et al. 1997; Abel, Bryan & Norman 2000, 2002; Bromm & Loeb 2004; Bromm & Larson 2004; Ciardi & Ferrara 2005; Yoshida et al. 2006; O'Shea & Norman 2007; Bromm et al. 2009) show that first stars are formed in $\sim 10^6\,M_\odot$ haloes if gas is condensed by H_2 cooling. It has been seen in these simulations that first stars are massive due to inefficient cooling (in the absence of metals and dust) and are formed in isolation. Recent work by Clark et al. (2010) shows that primordial gas is susceptible to fragmentation even with a small amount of turbulence. For metal-free gas, the only efficient coolants that can bring down the temperature below $\sim 10^4$ K are H_2 and HD. Gas will not fragment to form stars in their absence (Abel et al. 2000). Feedback processes can suppress the formation of molecular hydrogen (Haiman, Abel & Rees 2000).

Cooling due to molecular hydrogen in haloes having virial temperatures of $>10^4$ K can be suppressed through Lyman–Werner radiation emitted by a nearby star-forming galaxy. Such haloes therefore could be suitable for the growth of black holes (Dijkstra et al. 2008). Early fragmentation will not occur when H_2 cooling is suppressed either due to external or due to internal sources and will favour the formation of massive objects (Oh & Haiman 2002; Bromm & Loeb 2003; Begelman, Volonteri & Rees 2006). In the absence of molecular hydrogen cooling, gas can only cool through atomic line radiation. Wise, Turk & Abel (2008) performed cosmological simulations to study the collapse of protogalactic gas clouds cooled by only atomic lines and found that an object of $10^5\,M_\odot$ is formed in the centre of a metal-free halo. They also determined

⋆E-mail: latife@astro.rug.nl

that angular momentum transfer played a vital role in the formation of a massive object. Bromm & Loeb (2003) used smoothed particle hydrodynamics simulations to study the evolution of metal-free gas in the absence of H_2 cooling. Their results show that collapse is isothermal and fragmentation is not very efficient. As a result, one or two massive clumps of 10^6 $M_\odot$ are formed containing >10 per cent of gas. Regan & Haehnelt (2009b,a) carried out cosmological simulations and followed the dynamic evolution of metal-free haloes cooled by atomic line radiation and found that isothermal collapse leads to the formation of a self-gravitating stable disc at the centre of a halo.

Massive black holes can only form in atomic cooling haloes (Abel et al. 2000) with virial temperatures greater than 10^4 K. Self-gravitating gas can form black holes through direct collapse if it is cooled down to a small fraction of the virial temperature (Begelman & Shlosman 2009). Various other ways have been suggested for the formation of black holes (Rees 1978; Haiman 2004a,b; Portegies Zwart et al. 2004; Djorgovski et al. 2008; Devecchi & Volonteri 2009). Gas in primordial haloes can cool through atomic line radiation and collapses isothermally to form a 10^4–10^6 $M_\odot$ object if the temperature remains as high as 10^4 K (Spaans & Silk 2006). These authors found that trapping Lyman α photons stiffens the equation of state (EOS) and raises the temperature above 10^4 K. The fraction of molecular hydrogen is almost zero at such higher temperatures.

Trapping Lyman α photons increases the Jeans mass, and fragmentation is likely to be inhibited. The impact of Lyman α pressure on the accretion of first stars has been studied by McKee & Tan (2008). They found that it cannot effect the overall infall except in polar regions of 20–30 $M_\odot$ stars. The key assumption in most models for the formation of massive objects through direct collapse is that gas must avoid fragmentation, otherwise it might form low-mass Population III stars. Hence, quenching the formation of H_2 will be necessary. The model by Spaans & Silk (2006) for the formation of pre-galactic black holes requires no explicit mechanisms for the destruction of H_2 as trapping of Lyman α photons keeps the gas H_2 free (also see Schleicher, Spaans & Glover 2010). Motivated by their model, we have performed 3D cosmological simulations that include trapping effects of Lyman α photons and compared our results with previous work (atomic and H_2 cooling cases). The only assumption for this model is that the halo is metal free. The metal distribution is generally inhomogeneous and metal enrichment has not proceeded very far at higher redshifts. Pockets of metal-free gas can exist thus until a redshift of 6 (Trenti, Stiavelli & Michael Shull 2009).

The primary aim of this research is to follow the collapse of a (close-to) zero metallicity halo and to explore whether it fragments into a multiple system or forms a massive object without fragmenting. We carry out high-resolution cosmological simulations that have a dynamic range of $\sim 2 \times 10^5$ in linear scale and study the impact of thermodynamics on the collapse of primordial gas. We present in this paper three sets of high-resolution cosmological simulations with different physics ingredients. In the first case, we add atomic cooling assuming that there is a UV background that suppresses molecular hydrogen formation. In the second set of simulations, we include cooling due to molecular hydrogen to see how it affects the process of collapse. In the third suite of simulations, we assess the influence of Lyman α photon trapping on the formation of primordial objects. We compare the results of the Lyman α trapping case with atomic and molecular hydrogen cooling cases. For the case of Lyman α trapping, we assume that no molecular hydrogen formation takes place at temperatures above the collision break-up energy of H_2. Also, even small amounts of dust, if present, can absorb and re-emit the Lyman α photons at much lower frequencies (Haiman & Spaans 1999). So, we assume zero dust abundance.

Our paper is organized as follows. In Section 2, we describe the simulation set-up and numerical methods used in this paper. In Section 3, we discuss different heating and cooling mechanisms that we included in our simulations. Finally, in Section 4, we discuss the results obtained with our simulations and present our conclusions.

2 SIMULATIONS

We are using the code FLASH3 (Fryxell et al. 2000). FLASH is a module-based, Eulerian adaptive mesh refinement (AMR), parallel simulation code which can solve a broad range of astrophysics problems. The Message-Passing Interface library is used to get portability and scalability on many different parallel systems. It makes use of the PARAMESH library to handle a block-structured adaptive grid, to add higher resolution depending upon the user's defined refinement criteria. For hydrodynamic calculations, we use the directionally split piecewise-parabolic method (PPM; Colella & Woodward 1984) and inside shock waves we use the HLLE solver. PPM is favoured over other methods due to its higher order accuracy and its ability to sharpen shocks and contact discontinuities as it does not use artificial viscosity. In order to calculate the evolution of dark matter, FLASH uses an N-body particle mesh technique and couples it to the hydrodynamics. The gravity solver used in FLASH is the oct-tree-based multigrid Poisson solver developed by Ricker (2008).

We take a 3D box of 10 Mpc (comoving) on each side. In order to simulate the evolution of dark matter, we are initializing 2.6×10^6 particles. We use the COSMICS (grafic) package developed by Bertschinger (1995) to introduce Gaussian random field cosmological initial conditions. As motivated by inflation, the density perturbations are assumed to be isotropic, homogeneous and Gaussian. We use standard parameters from the *Wilkinson Microwave Anisotropy Probe* 5-yr data ($\Omega_\mathrm{m} = 0.2581$, $H_0 = 72\,\mathrm{km\,s^{-1}\,Mpc^{-1}}$, $\Omega_\mathrm{b} = 0.0441$) with a value of $\sigma_8 = 0.8$. We use periodic boundary conditions for both gravity and hydrodynamics.

We run the COSMICS package to create Gaussian random initial conditions and select the set of initial conditions having the highest density peak. We find the location of the highest density peak and shift it to the centre of the box. In the region of 1 Mpc around the centre of the box, we initialize our simulation with a high level of resolution, which corresponds to 512^3 grid cells. The rest of the box is set to a resolution of 128^3 cells. We start the simulation at redshifts ranging from $z = 50$ to 70 for different sets of Gaussian random field initial conditions with higher and lower density peak haloes. We select a massive halo and zoom in with the FLASH refinement criteria. As adding higher levels of uniform refinement within the region of interest becomes a computationally demanding task, we exploit the AMR technique to add dynamic levels of refinement. We add eight additional dynamic levels of refinement using specific density threshold criteria. This gives us 15 levels of refinement in total. The effective resolution in the region of interest is $\sim 2 \times 10^5$ in linear scale (i.e. dynamic range). The virial mass of the system is $\sim 3 \times 10^9$ $M_\odot$ and the virial temperature is $\sim 10^5$ K [$T_\mathrm{vir} = 10^4 \times (M_\mathrm{vir}/M_\odot)^{3/2}\,(1 + z_\mathrm{vir}/10)$]. The collapse happens at a redshift of 10. In the case of molecular hydrogen cooling, the Jeans mass reduces as gas cools to lower temperatures and collapses to higher densities compared to the other simulations, so we add an additional dynamic refinement level to resolve the Jeans mass (maximum refinement in this is 16 levels). Our refinement

criteria are good enough to resolve shock waves and they also ensure the fulfilment of the Truelove criteria stating that the Jeans length should be resolved by at least four cells (Truelove et al. 1997). In this way, we avoid artificial fragmentation caused by density perturbations created during discretization of the grid. The top level hierarchy of refinement levels helps in even greater precision.

3 PHYSICS INCLUDED

3.1 Cooling

Cooling is an important process in the formation of structures, such as stars and galaxies. It is crucial to understand the physics of cooling in primordial gas in order to study the formation of the first objects. Adequate amounts of gas have to gather in dark matter haloes to form structures. Cooling becomes efficient when the cooling time $t_{\rm cool} = 3nkT/2\Lambda$ becomes less than the free-fall time $t_{\rm ff} = \sqrt{3\pi/32G\rho}$, where n is the number density, ρ is the mass density and Λ is the cooling rate. Under this condition gas cools, collapses and can fragment. Mass scales of fragments are determined by the Jeans mass $M_{\rm J} \approx 10^6\,{\rm M}_\odot\ (T/10^4\,{\rm K})^{3/2}$ (for typical densities of $10^4\,{\rm cm}^{-3}$) which depends on the thermodynamics of the gas. Gas cannot cool below 8000 K if it is cooled by only atomic line radiation. Consequently, the Jeans mass remains $>10^5\,{\rm M}_\odot$ and fragmentation to lower mass scales is inhibited. In order to induce fragmentation of lower mass scales, gas should be cooled down to lower temperatures. Introduction of molecular hydrogen and HD cooling can lower the gas temperature down to $\sim$100 K and reduce the Jeans mass to $\sim 10^3\,{\rm M}_\odot$. Fragmentation at lower than the Jeans scale is prohibited as gas becomes pressure supported.

The net cooling function of a gas is a combination of processes, such as line radiation, photoionization, Compton scattering, bremsstrahlung, radiative recombination, etc. The cooling function strongly depends on the composition of the gas. The primordial composition of the gas is dictated by big bang nucleosynthesis. We take a primordial composition for the gas with 75 per cent hydrogen and 25 per cent helium by mass. In metal-free gas, the dominant cooling process is atomic line cooling. As primordial gas is metal free, we are implementing a zero metallicity cooling function by Sutherland & Dopita (1993). At higher temperatures of 10^6–10^8 K, cooling is due to free–free transitions. For temperatures between 10^4 and 10^6 K, cooling is mainly due to H I and H II Lyman α.

Evolution of primordial density fluctuations is controlled by the ability of gas to cool down to low temperatures. The temperature of gas remains $\approx$8000 K in the absence of H_2 and HD (Galli & Palla 1998) due to high excitation energies of primordial gas atoms. In the absence of metals, H_2 cooling is crucial to form stars in $T_{\rm vir} > 10^4$ K haloes. Vibrational and rotational modes of H_2 can be excited at low temperatures of $\sim$500–1000K. Trace amounts of molecular hydrogen can form via gas phase reactions in the post-recombination era (Peebles & Dicke 1968). We use the Galli & Palla (1998) cooling function to include cooling due to molecular hydrogen. We take a universal abundance of H_2, i.e. 10^{-3}. The zero metal cooling function is shown in Fig. 1; details can be found in Galli & Palla (1998) and Peebles & Dicke (1968).

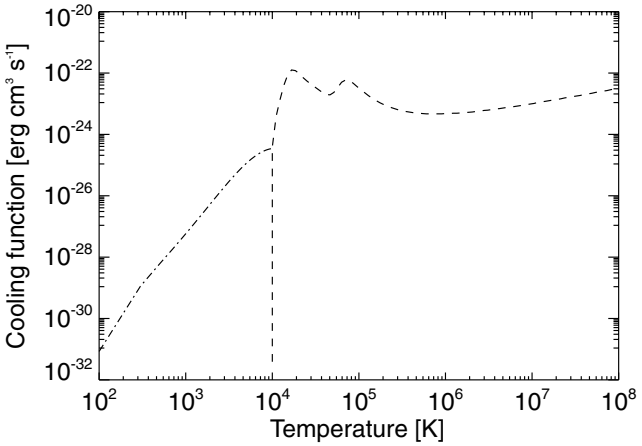

Figure 1. Cooling function for zero metallicity. The dashed line shows the zero metal cooling function while the dash–dotted line depicts the contribution due to molecular hydrogen.

3.2 Variation in the equation of state

The EOS plays a vital role in structure formation. Fragmentation of gas clouds is strongly dependent on the polytropic EOS (Li, Klessen & Mac Low 2003). The relation of the polytropic index of the EOS (γ) to the logarithmic derivatives of the heating and cooling function implicitly includes radiative transfer effects (Spaans & Silk 2000). Under conditions of thermal equilibrium, by balancing the heating and cooling terms, the polytropic exponent which measures the compressibility of gas can be written as (Scalo & Biswas 2002)

$$\gamma = 1 + \frac{{\rm d}\log T}{{\rm d}\log \rho}. \quad (1)$$

Spaans & Silk (2006) have studied the effect of trapping Lyman α photons on the polytropic EOS for primordial haloes. They found that trapping Lyman α photons stiffens the polytropic exponent significantly above unity. Consequently, the Jeans mass is boosted and fragmentation is halted.

As the collapse proceeds, gas becomes optically thick. The escape probability of Lyman α photons, which perform a random walk in both space and frequency, is reduced and ultimately photons are trapped inside the cloud. If the photon traveltime becomes larger than the free-fall time, the radiative energy is redeposited inside the gas and consequently cooling is suppressed and the temperature of the gas becomes $\geq 10^4$ K. The formation of molecular hydrogen will not take place as it is collisionally dissociated at temperatures higher than 8000 K. Rees & Ostriker (1977) have studied the influence of trapping radiation on collapsing gas clouds and concluded that trapping of Lyman α photons can inhibit fragmentation. They also mentioned that trapped radiation would exert pressure which is half of the pressure required to support the cloud and will not halt the overall collapse. Radiation pressure produced by trapping of Lyman α photons can considerably constrain the efficiency of star formation (Oh & Haiman 2002).

At optical depths $\tau_0 > 10^7$, the photon escape time $t_{\rm ph}$ becomes larger than $t_{\rm ff}$. Due to the weak dependence of $t_{\rm ph}$ on the number density ($t_{\rm ph} \propto n^{-1/9}$), the photon escape time remains longer than the free-fall time ($t_{\rm ph} \propto n^{-1/2}$) during the collapse (Spaans & Silk 2006). The number of photons that is trapped at the line centre thus increases and the emission of Lyman α photons from the core tends to zero. Consequently, trapping becomes more effective during the collapse. The scattering of Lyman α photons during the collapse can introduce extra pressure which slows down the process of collapse. This changes the density of trapped Lyman α photons and induces fluctuations in the EOS which are not well captured in our case. A temporary softening of the EOS would favour fragmentation, and our approach therefore gives an upper limit on the effect of Lyman

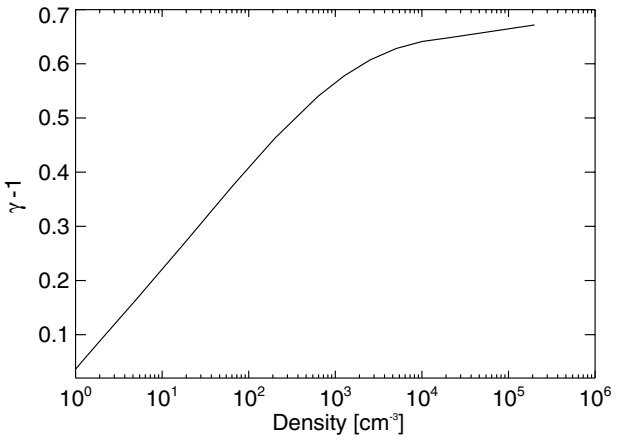

Figure 2. Variation of γ with density. The change in polytropic index ($\gamma - 1$) is plotted as a function of the number density (cm^{-3}) of the gas. The figure shows the stiffening of the EOS by trapping Lyman α photons.

α trapping. The minimum hydrogen column density required for the trapping is $N_{\rm H} = 10^{21}\,\mathrm{cm}^{-2}$.

By trapping Lyman α photons, the polytropic index γ increases from 1.01 to 1.50 for hydrogen number densities of 1–$10^5\,\mathrm{cm}^{-3}$ (Spaans & Silk 2006). We found that high columns in our case stiffen the EOS at lower density values than mentioned by Spaans & Silk (2006). Due to high columns, gas becomes opaque at lower number densities and causes more efficient trapping of Lyman α photons. Therefore, we have modified Spaans & Silk (2006) criteria for the change in polytropic index to include high column opacity effects. Their model is based on analytical results and does not take into account the resolution constraints. We use the formula given below to implement the change in the polytropic exponent of the EOS γ:

$$\gamma - 1 \approx -\frac{\frac{1}{2} + \frac{7}{18} B n_1^{7/18}}{\log(C n_1^{0.5}) + B n_1^{7/18}}, \quad (2)$$

where the value of $B \approx 0.47\,\mathrm{cm}^{7/6}$, $C \approx 10^{-34}\,\mathrm{cm}^{3/2}$ and n_1 is 100 times the number density. Fig. 2 illustrates the stiffening of the EOS as a function of number density. It can be seen from the figure that gas remains close to isothermal up to 10 cm^{-3} and at higher densities opacity effects stiffen the value of γ well beyond unity. An increase in the value of γ enhances temperature well above 10^4 K. Even a value of $\gamma \sim 1$ should already be sufficient to halt fragmentation and will lead to isothermal collapse. Cooling due to helium becomes important at temperatures higher than 5.0×10^4 K. Above $10^3\,\mathrm{cm}^{-3}$, opacity effects due to thermal bremsstrahlung trapping come into play and cooling continues to be suppressed. A value of $\gamma \geq 4/3$ leads to an adiabatic collapse. Helium opacity effects can be included by making corrections to equation (2). Details can be found in Spaans & Silk (2006).

4 RESULTS

Our simulations show that density perturbations decouple from the Hubble flow and start to collapse through gravitational instability. The fate of these perturbations depends on the cooling and dynamical time-scales. At low densities, cooling is very inefficient. We see in our simulations that initially the gas is shock heated at low densities ($\leq 10^{-1}\,\mathrm{cm}^{-3}$). Virialization processes transform gravitational potential energy into kinetic energy of the gas and dark matter. As dark matter cannot dissipate, for gas this energy is converted into internal energy through shocks which raises the temperature of the gas to the virial temperature. We start with an adiabatic EOS as perturbations in the intergalactic medium are adiabatic in nature. According to linear perturbation theory, the EOS should show a power-law behaviour in the low density regime (Hui & Gnedin 1997; Springel & Hernquist 2002), given by the equation

$$T = T_0(\rho/\rho_0)^{\gamma-1}, \quad (3)$$

where T_0 and ρ_0 are the cosmic mean density and temperature, respectively. Our results agree with this analytical temperature density relation for the intergalactic medium.

At a redshift of 15, gas begins to cool and collapses in the gravitational potential provided by the dark matter. At densities of the order of 10^4 times the mean density of the Universe, cooling due to atomic lines (hydrogen and helium) becomes very efficient and gas becomes isothermal with a value of γ of unity. Gas continues to collapse if the cooling time is smaller than the dynamical time. We have investigated the dynamic and thermal evolution of primordial gas which is cooled or heated and collapses under different post-shock heating mechanisms. In the next subsections, the results are discussed for each case individually. We use the isovolume-connected components finding algorithm implemented in the visualization program Visit (Childs et al. 2005) to find fragments. For a given density threshold, we find the fragments and calculate their masses.

4.1 Atomic line cooling

Metal-free haloes with virial temperatures of $>10^4$ K and no Lyman α trapping can be prone to molecular hydrogen formation if not irradiated by an intense UV flux. There may exist some halo pairs where molecular hydrogen is photodissociated by the Lyman Werner radiation of the other halo (Dijkstra et al. 2008). Recent calculations by Shang, Bryan & Haiman (2010) indicate that specific intensities required to suppress the formation of molecular hydrogen are three to 10 times lower than the previous estimates of $J_{\rm crit} \sim 1000$ in units of $10^{-21}\,\mathrm{erg\,cm^{-2}\,s^{-1}\,Hz^{-1}\,sr^{-1}}$. Consequently, the population of such haloes is enhanced by a factor of $\approx 10^3$. We assume that the halo is metal free and illuminated by intense UV flux. Hence, the formation of H_2 does not take place. Initially, gas heats up to its virial temperature. When the cooling time becomes less than the dynamical time, it begins to cool and collapse in dark matter potentials. As cooling due to Lyman α photons is very efficient, the gas cannot virialize by gaining internal energy, so its kinetic energy must be increased to reach virial equilibrium. Consequently, during virialization the gas becomes turbulent. It continues to cool and collapse into the centre of a halo.

Gas in the halo collapses up to densities of a few times $10^5\,\mathrm{cm}^{-3}$. It fragments into two massive clumps of 2.6×10^6 and $1.3 \times 10^6\,\mathrm{M}_\odot$ as shown in Fig. 3. Collapse is nearly isothermal and gas in the halo is cooled down to only a small fraction of the virial temperature. Isothermal behaviour is depicted in the temperature slice in Fig. 4. The temperature remains around ~8000 K. The value of the polytropic index remains close to 1. Isothermal collapse prevents it to fragment into smaller clumps and the Jeans mass is $2 \times 10^5\,\mathrm{M}_\odot$.

The gas passes through different phases during collapse which are shown in the temperature–density phase diagram in Fig. 5. It is initially shock heated at low densities and subsequently cooled by atomic line cooling. Most of its mass lies at low densities and only a small fraction (<1 per cent) is cooled and collapsed into clumps. It falls into the centre of a halo through filaments, and the direction of

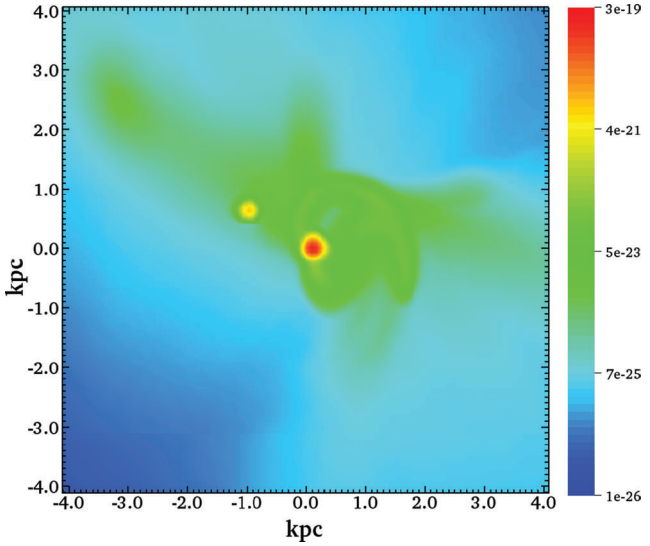

Figure 3. Density slice through the centre of a halo for the atomic cooling case. Values corresponding to each colour are shown in a colour bar, where the blue colour represents the lowest density and red represents the highest density. Distance scales are in comoving units. Here, 1 kpc in comoving units corresponds to 106 pc in proper units.

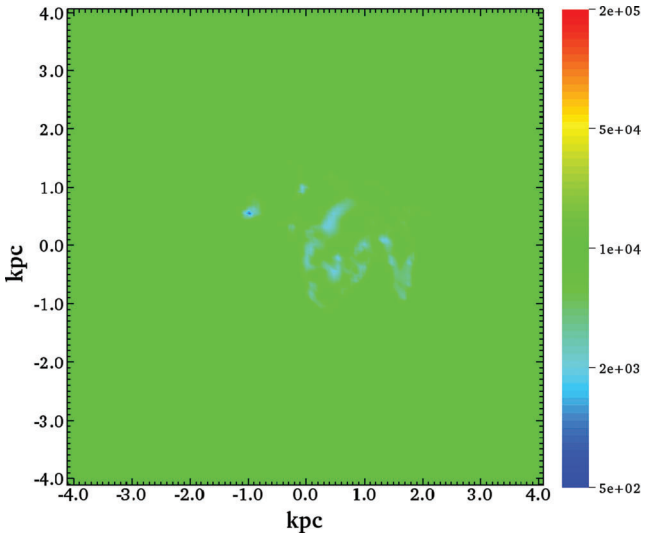

Figure 4. Temperature slice through the centre of a halo for the atomic cooling case. The figure shows the temperature corresponding to the density slice of Fig. 3. The blue colour represents the lowest temperature and red represents the highest temperature.

the flow is shown by velocity vectors in Fig. 6. The typical velocity is around 100 km s^{-1}. We also examined the entropy of gas in the halo and found that it is 10^{-2} keV cm^{-2}.

Our results are in agreement with previous results (Bromm & Loeb 2003; Wise et al. 2008). We do not see disc formation in our case as mentioned by Regan & Haehnelt (2009a). The reason for this disagreement could be due to a difference in resolution. We do not exclude the possibility of disc formation which may form after collapse. Inefficient fragmentation of a halo for isothermal collapse is according to the expectation of theoretical models.

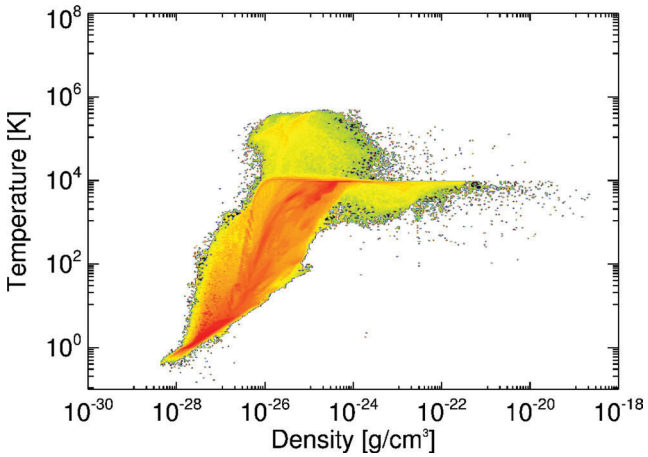

Figure 5. Density–temperature phase diagram for the atomic cooling case. Temperature is plotted against volume-weighted density in filled colour contours by merging an adaptive grid into a uniform grid, where the red colour shows the highest mass and purple shows the lowest mass.

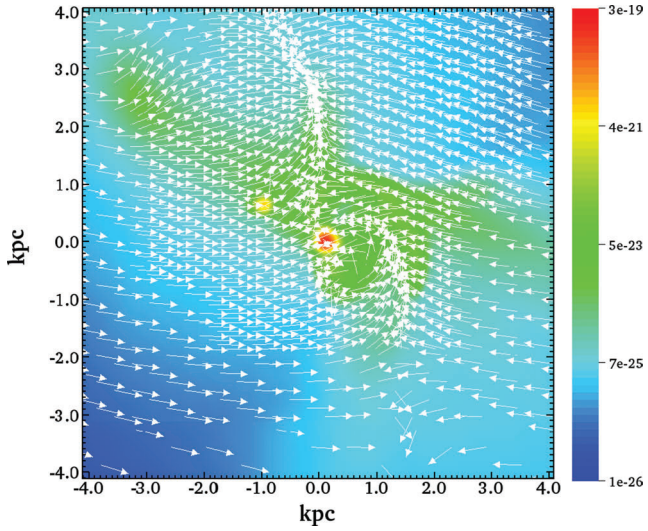

Figure 6. Velocity vectors are overplotted on a density slice for the atomic cooling case. Velocity vectors are indicated by white colour arrows. The head of the arrows indicates the direction of flow.

4.2 Molecular hydrogen cooling

Adding molecular hydrogen cooling enhances the low temperature cooling and increases the fragmentation. We see that gas is heated up to its virial temperature by shock waves at lower densities and subsequently cools by atomic line cooling. At densities higher than 1 cm^{-3}, cooling due to molecular hydrogen comes into play and lowers the temperature down to ∼100 K. During collapse, it passes through different phases; its multiphase behaviour is shown in the temperature–density phase diagram in Fig. 7. Most of the gas lies at low densities and only a small fraction (<1 per cent) is cooled and collapses into minihaloes.

The EOS is softened due to H_2 cooling and the value of the polytropic index is lowered to less than unity. Hence, the Jeans mass is reduced. A density slice is shown in Fig. 8. H_2-cooled gas is seen at the intersection of filaments. The gas collapses into six minihaloes in contrast to the Lyman α trapping case, where gas does not collapse into minihaloes. Their masses are 2×10^6, 8×10^5, 8×10^5, 3×10^5, 1×10^5 and 3.4×10^5 $M_\odot$. Only two of the minihaloes

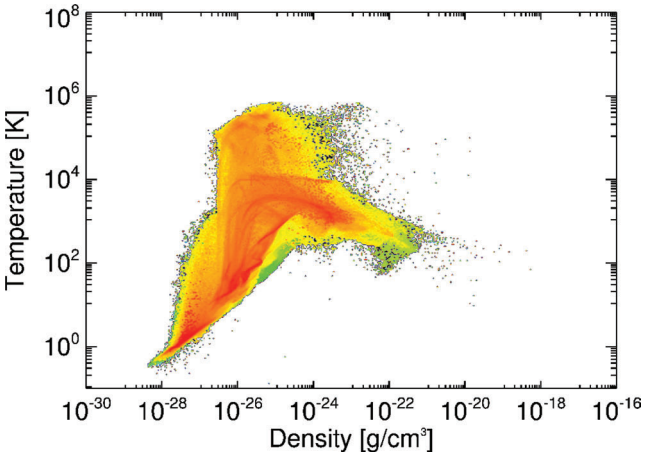

Figure 7. Density–temperature phase diagram for the molecular cooling case. Temperature is plotted against the volume-weighted density in filled colour contours by merging an adaptive grid into a uniform grid, where the red colour shows the highest mass and purple shows the lowest mass.

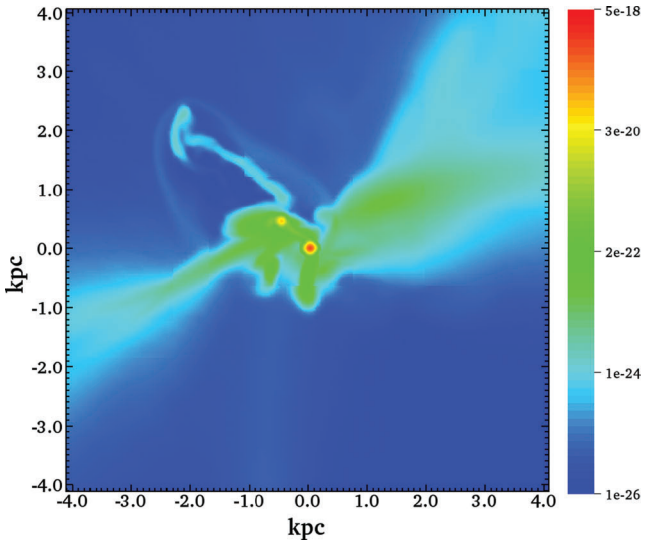

Figure 8. Density slice through the centre of a halo for the molecular cooling case. Values corresponding to each colour are shown in the colour bar, where the blue colour represents the lowest density and red represents the highest density. Distance scales are in comoving units. Here, 1 kpc in comoving units corresponds to 106 pc in proper units.

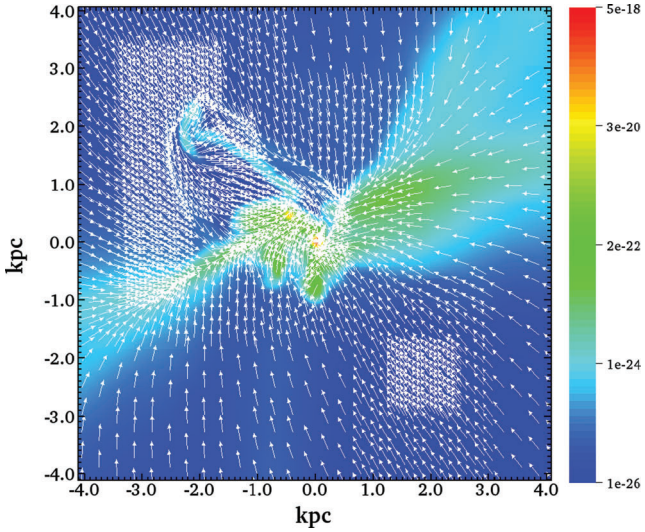

Figure 9. Velocity vectors are overplotted on the density slice for the molecular hydrogen cooling case. Velocity vectors are indicated by white colour arrows. The head of the arrows indicates the direction of flow.

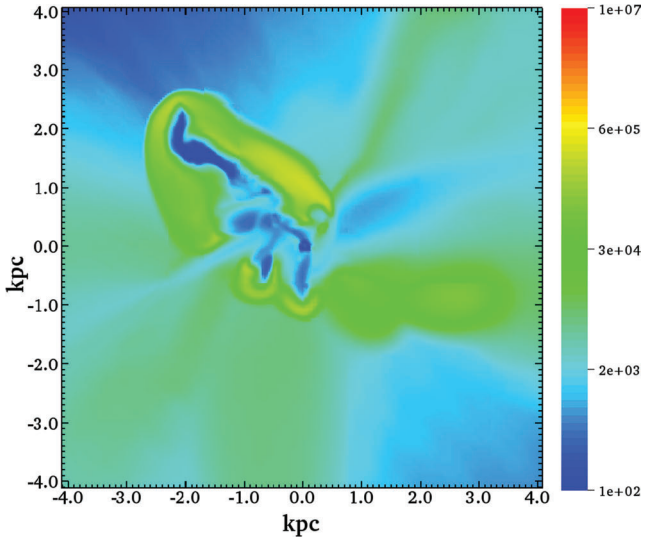

Figure 10. Temperature slice through the centre of a halo for the molecular hydrogen cooling case. The figure shows the temperature corresponding to the density slice of Fig. 8. The temperature of fragments is close to 100 K which can be seen in a blue colour in the plot.

are visible in the slice. Their sizes are significantly smaller than the other cooling cases. The Jeans mass is reduced to $\sim 10^3\,M_\odot$ and the gas collapses to densities of a few times $10^6\,cm^{-3}$. The gas becomes turbulent during virialization and falls into the centre of a halo through cold streams as seen in Kereš et al. (2009), Fardal et al. (2001), Dekel et al. (2009), Greif et al. (2008) and Wise & Abel (2007). The density is $\sim 10\,cm^{-3}$ and temperature is ~ 300 K in these streams. The direction of flow is presented in Fig. 9. The temperature of the minihaloes is around 100 K and is shown in Fig. 10. Shock-heated gas is seen in the vicinity of the minihaloes and the penetration of cold flows is even more prominent in this plot. The introduction of H_2 cooling has significantly reduced the entropy of the gas down to 10^{-5} keV cm^{-2}. Entropy is low in the minihaloes, higher in outskirts and even boosted in shocks (10^2 keV cm^{-2}).

4.3 Lyman α trapping

It is generally assumed that gas, even though very optically thick ($\tau > 10^7$) to the scattering of Lyman α photons, can cool efficiently through Lyman α because radiation leaks out in the line wings. High columns of neutral atomic gas make the gas so optically thick that photon traveltime exceeds the $t_{\rm ff}$. So, using the effectively optically thin cooling rate is not a good approximation above $10^{20}\,cm^{-2}$. Consequently, the EOS stiffens as explained in the previous section and cooling is suppressed. Gas remains almost optically thin up to densities on the order of $10\,cm^{-3}$. At densities of $\geq 10^2\,cm^{-3}$, it becomes opaque enough that cooling due to Lyman α photons is quenched. When the gas density exceeds $10^3\,cm^{-3}$, at typical columns of the order of $10^{23}\,cm^{-2}$, the two-photon continuum channel is shut down and photons are absorbed by neutral hydrogen in the surroundings

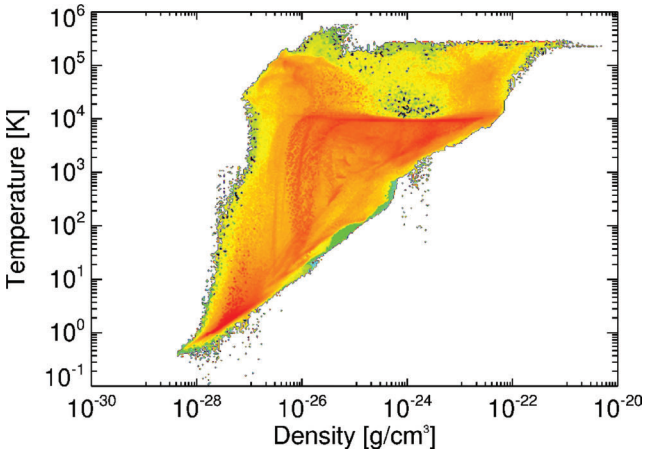

Figure 11. Density–temperature phase diagram for the Lyman α trapping case. Temperature is plotted against volume-weighted density in filled colour contours by merging an adaptive grid into a uniform grid, where the red colour shows the highest mass and purple shows the lowest mass.

(Spaans & Silk 2006). Under these conditions, the halo collapses adiabatically to form a massive object.

Gas is initially shock heated at low densities, becomes isothermal at densities of $\sim 1\,\mathrm{cm}^{-3}$, while at densities of $\geq 1\,\mathrm{cm}^{-3}$ the EOS is stiffened because of Lyman α trapping. This multiphase behaviour is depicted in the density–temperature phase diagram in Fig. 11. Most of the gas is lying at low densities and only a small fraction (<1 per cent) collapses to high densities. Gas in the halo becomes turbulent during virialization and is segregated according to its angular momentum distribution (low angular momentum gas falls into the centre). Hence, the collapse happens in the centre of a halo. An object of a mass of $4.0 \times 10^6\,\mathrm{M}_\odot$ is formed at the intersection of filaments which may lead to a massive object, i.e. an intermediate-mass black hole (IMBH). We see signs of a cold flow, which has already been seen in numerical simulations by Dekel et al. (2009), Kereš et al. (2009) and Fardal et al. (2001). Baryons accumulate into the centre of a halo via a two-phase medium by the entrance of cold flow streams through the shock-heated medium.

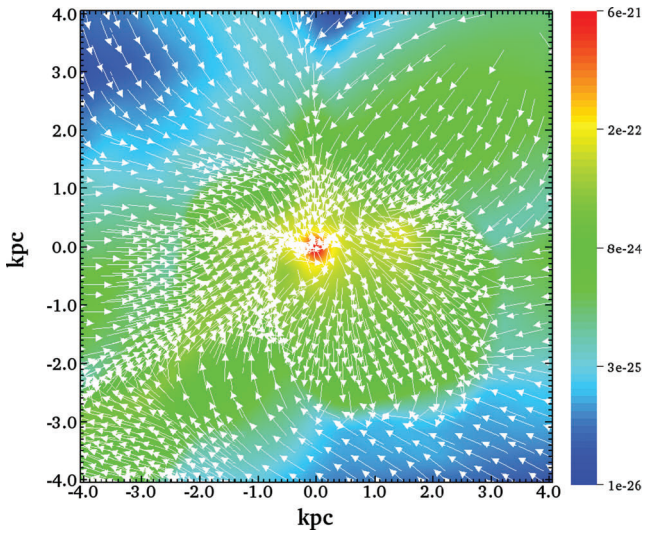

Figure 12. Velocity vectors are overplotted on a density slice for the Lyman α trapping case. Velocity vectors are indicated by white colour arrows. The head of the arrows indicates the direction of flow.

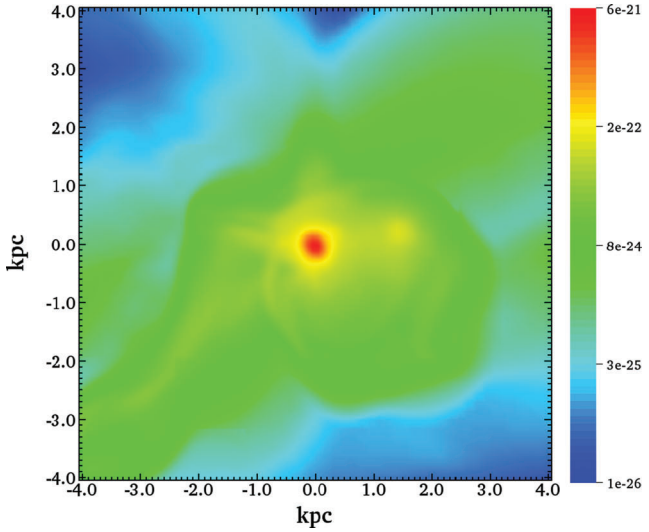

Figure 13. Density slice through the centre of a halo for the Lyman α trapping case. Density is shown in rainbow colours where red represents the highest density and purple represents the lowest density. Distance scales are in comoving units. Here, 1 kpc in comoving units corresponds to 106 pc in proper units.

These flows also explain the observed Lyman α blob morphologies (Dijkstra & Loeb 2009). The direction of flow is shown by velocity vectors in Fig. 12. The values of the velocity in the centre of the halo are about 100 $\mathrm{km\,s}^{-1}$ which are typical values for such objects.

The morphology of the object is shown in Fig. 13. Diffuse hot gas is visible in the vicinity of the object. Contraction of gas is halted and the Jeans mass is boosted due to Lyman α trapping. Diffuse gas may feed the central object during later stages of collapse. The halo does not collapse to high densities (few $\times\ 10^3\,\mathrm{cm}^{-3}$ in this case) as compared to other cases because of suppressed cooling. The temperature is enhanced due to trapping of Lyman α photons as depicted in Fig. 14. It is $\geq 10^4$ K in the centre of the halo and even higher in the shock fronts. Trapping of Lyman α photons keeps

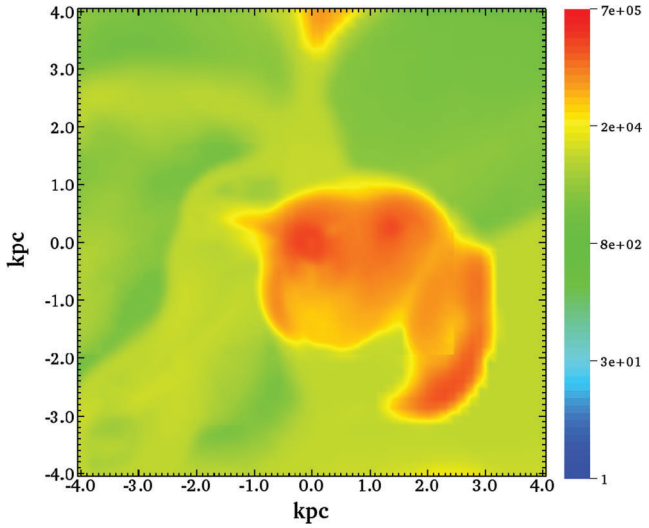

Figure 14. Temperature slice through the centre of a halo for the Lyman α trapping case. The figure shows the temperature corresponding to the density slice of Fig. 13. The temperature of the object is high compared to the atomic cooling case. Distance scales are in comoving units.

the gas H_2 free, as collisional dissociation and charge exchange at a temperature above 5000 K destroy H_2 formation (Oh & Haiman 2002). Spaans & Silk (2006) have confirmed through models that column densities in the range of 10^{22}–10^{25} cm^{-2} will be sufficient to self-shield the gas even from X-rays. This puts our arguments in favour of suppressed fragmentation on sounder footing. The inability of gas to fragment makes such haloes prone to the formation of massive objects. The collapse is never halted but only delayed in the case of Lyman α trapping as compared to other simulations (molecular hydrogen and atomic cooling). This delay is caused by the enhanced radiation pressure as more work needs to be done on the gas. Entropy of gas is increased as a consequence of Lyman α trapping up to 0.1 keV cm^2. It is even higher (10 keV cm^2) in shocks. We see that trapping of Lyman α photons increases the entropy of gas which is close to the lower limit for entropy in simulations of galaxy groups and clusters with radiative cooling (Borgani et al. 2005). We do not include feedback effects which may inject extra energy and raise the entropy of the gas to even higher values.

5 DISCUSSION AND CONCLUSIONS

We have probed the influence of thermodynamics on the formation of the first objects in primordial gas. We have introduced the impact of Lyman α trapping, atomic and molecular hydrogen cooling, and performed cosmological 3D simulations down to a redshift of 8.4 using the AMR code FLASH. We exploited the AMR technique to add dynamic levels of refinement wherever required, so that our resolution is sufficient to resolve the most essential physics. We have assumed that haloes are metal free. Pockets of metal-free gas can exist until a redshift of $\sim$6 (Trenti et al. 2009).

Line trapping of Lyman α photons stiffens the EOS and enhances the Jeans mass. We noticed that Lyman α photons trapped in haloes inhibit cooling below $\sim 10^4$ K; consequently, gas fragmentation is halted and a massive object is formed at the centre of a halo. We performed a set of simulations with one higher level of refinement for this case and found the same results as mentioned before. As trapping continues, formation of H_2 will be suppressed and a halo will collapse adiabatically. The outcome of the object depends on

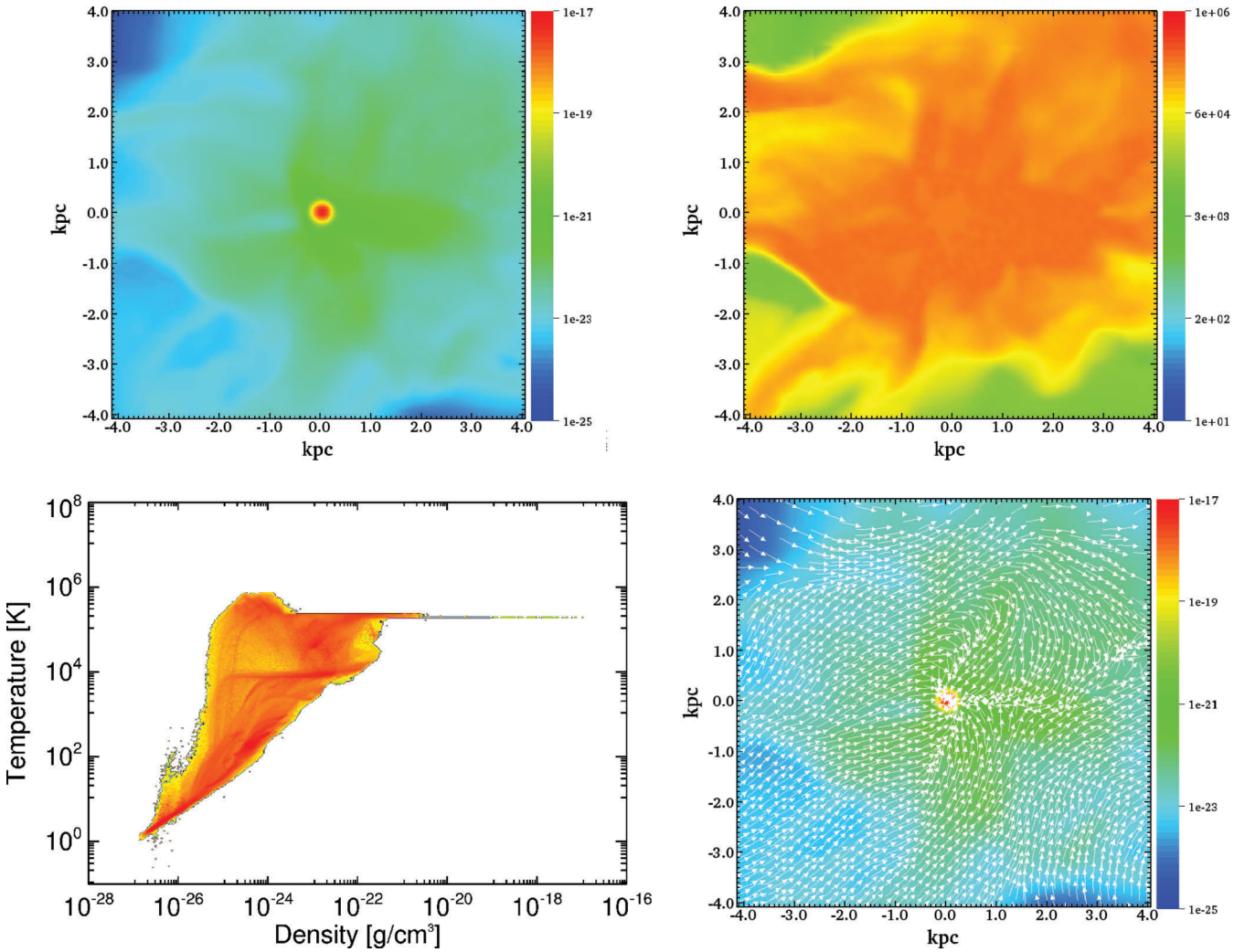

Figure 15. A higher density peak halo for the Lyman α trapping case. The top-left panel shows the density slice through the centre of a halo. The temperature slice corresponding to the density slice is depicted in the top-right panel. The bottom-left panel shows the phase diagram. The flow of gas is seen in the bottom-right panel. Values corresponding to colours are shown in the colour bars. Distance scales are in comoving units. Here, 1 kpc in comoving units corresponds to 53 pc in proper units.

how fast and efficient it accretes mass. It can directly collapse into a black hole or a supermassive star as an interim stage. We conclude that trapping of Lyman α photons during gas cloud collapse provides a venue for the formation of black holes, particularly when there is modest background UV flux to suppress molecular hydrogen cooling. Radiative transfer effects thus play a crucial role in the formation of massive objects observed at $z > 6$.

Our results are only valid for metal-free haloes. The addition of trace amounts of metals can change the scenario for Lyman α trapping. If dust is present then the gas temperature is lowered, and the EOS softened, due to absorption and IR re-emission of Lyman α photons. Haloes might have been pre-enriched by the heavy metals formed in and dispersed through supernovae explosions (Johnson, Greif & Bromm 2008; Greif et al. 2010). Such a scenario would suppress the effectiveness of Lyman α trapping because dust would efficiently absorb the Lyman α photons and reradiate them in the far-infrared. As such, we again find an upper limit on the importance of Lyman α trapping. Still, if the medium is inhomogeneous, which it very likely is, then Lyman α may scatter off dense gas condensations without being absorbed by dust and thus remain trapped in a collapsing structure (Neufeld 1991; Haiman & Spaans 1999). Fragmentation of the gas is inevitable in the presence of dust and metals (Omukai, Schneider & Haiman 2008). Recent work by Schleicher et al. (2010) shows that after initial collapse, cooling may proceed through other atomic states in the presence of Lyman α trapping. It can soften the EOS to unity and lead to disc formation, which may or may not fragment to form a top-heavy stellar initial mass function. We have explored the important phase of Lyman α trapped haloes. Cosmological simulations should be performed to examine the effect of other cooling channels such as 2s–1s and 3–2 transitions in haloes that are optically thick to Lyman α photons.

For the atomic cooling case, we find that the halo collapses into one or two massive clumps. As long as H_2 cooling is suppressed, gas collapses isothermally and remains hot having temperature around 8000 K. Further fragmentation is unlikely. Therefore, such haloes are plausible candidates for the formation of IMBHs or supermassive stars at an intermediate stage. The formation of molecular hydrogen does not take place if internal or external UV radiation from the star-forming halo can suppress H_2 formation (Shang et al. 2010; Dijkstra et al. 2008). At densities of $>10^8\,\mathrm{cm}^{-3}$, molecular hydrogen may form due to 3-body reactions (Palla, Salpeter & Stahler 1983) in the absence of intense UV flux and may

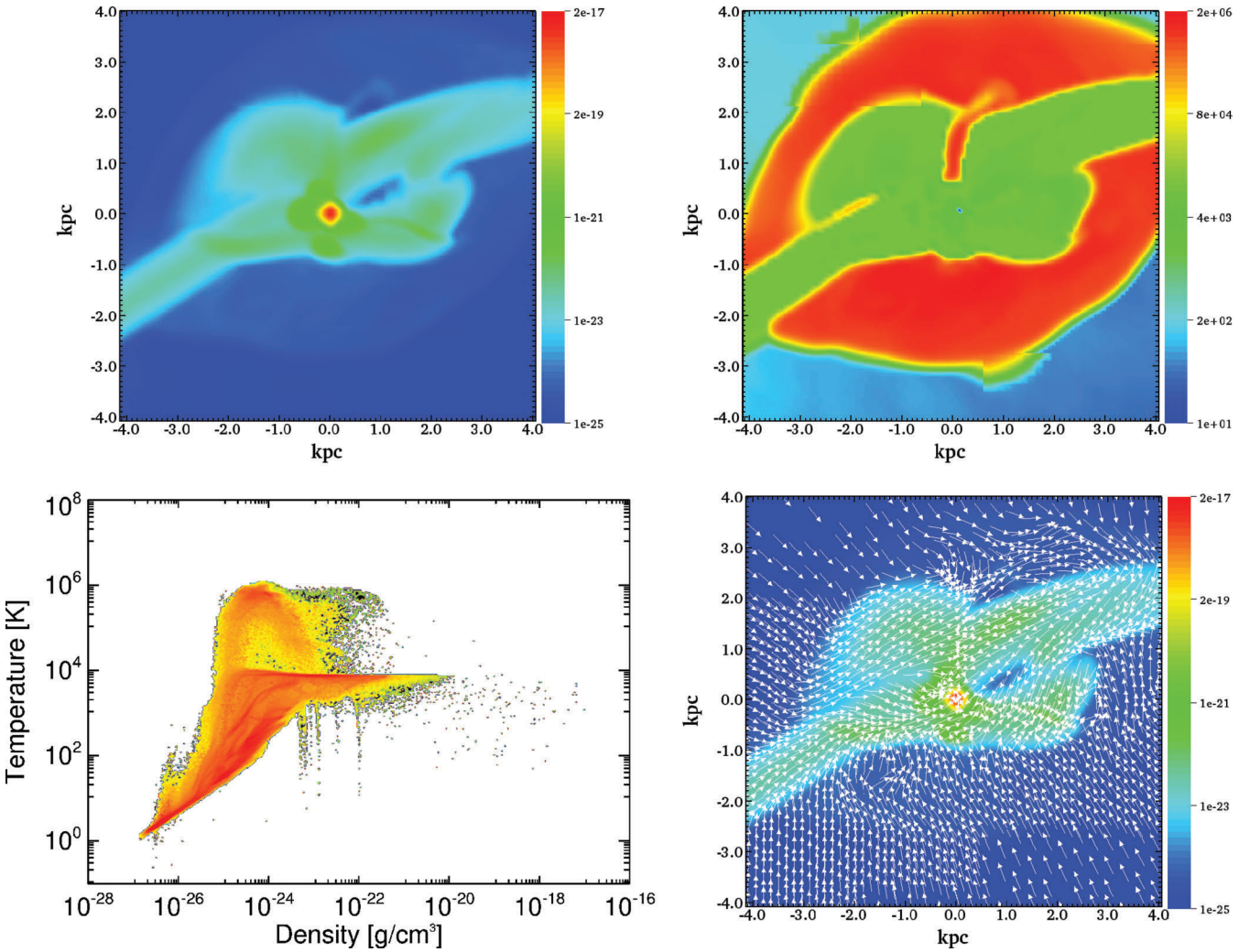

Figure 16. A higher density peak halo for the atomic cooling case. The top-left panel shows the density slice through the centre of a halo. The temperature slice corresponding to the density slice is depicted in the top-right panel. The bottom-left panel shows the phase diagram. The flow of gas is seen in the bottom-right panel. Values corresponding to colours are shown in the colour bars. Distance scales are in comoving units. Here, 1 kpc in comoving units corresponds to 53 pc in proper units.

induce fragmentation. The further fate of these objects should be explored through cosmological simulations by including detailed physics.

We have also performed simulations by selecting a high density peak halo. We noticed that in the higher density peak halo, the free-fall time becomes shorter and a halo collapses at about a redshift of 25. We followed the collapse down to a redshift of 18 and compared the results of atomic line cooling with the Lyman α trapping case. We find that the Lyman α trapped halo does not fragment irrespective of the high or low density peak in contrast to the atomic cooling case. Trapping of Lyman α photons keeps the gas hot ($T \geq 10^4$ K) and contraction of a halo is halted. The Jeans mass becomes higher and it does not fragment. The size of the fragment is larger than the atomic cooling case. The mass in a higher density peak halo is $5 \times 10^7\,M_\odot$. The mass of the object is not much higher than the atomic cooling case because more gas falls into the halo due to efficient atomic cooling and condenses. The density, temperature, phase diagram and velocity vectors for a higher density peak halo are shown in Fig. 15.

For the atomic cooling case, the morphology and thermodynamical properties of the clumps are similar in both higher and lower density peak haloes. The density, temperature, phase diagram and velocity vectors for a higher density peak halo are shown in Fig. 16. We find that the higher density peak halo fragments as in the lower density peak case. It is depicted in the density slice (zoomed in) in Fig. 17. Density contours are overplotted on the density slice and are compared with the Lyman α case. One can see that there is more structure in the atomic case as compared to the trapping case. We found that a clump surrounding the massive one is gravitationally bound and the mass is close to the Jeans mass. We also noticed that a smaller clump rotates around the massive one. The velocity field for the atomic cooling case (inner 2-kpc region) is shown in Fig. 18 and is compared with the Lyman α case. There is also divergence in the flow of gas corresponding to density contours. It supports our claim of fragmentation. The masses of the clumps in a higher density peak halo are $\sim 3 \times 10^7$ and $4.0 \times 10^5\,M_\odot$. These fragments will become even more prominent in higher resolution simulations.

In the case of molecular hydrogen cooling, the gas is cooled down to 100 K and collapses into minihaloes. The minihaloes formed via H_2 cooling are the potential sites for Population III star formation. Following the collapse becomes a computationally difficult task as the Jeans mass keeps dropping. We stop the simulation when the Truelove criterion is about to be violated. Adding higher resolution may help in fragmentation. Further fragmentation may occur at the higher densities due to an enhanced fraction of the molecular hydrogen formed through 3-body reactions. We did not include the HD cooling which is a very efficient coolant around 100 K. Introduction of the HD cooling will cool the gas below 100 K and may enhance fragmentation.

We have performed a set of simulations for the higher density peak H_2-cooled halo and compared it with the lower density peak halo. We find that the gas collapses into minihaloes. Efficient fragmentation of the H_2-cooled gas halo occurs regardless of being in low or high density peak haloes. The thermodynamical properties of the minihaloes are very similar in both cases. The difference in the collapse time of the higher and lower density peak haloes is the same as mentioned for the atomic cooling case. The density, temperature, phase diagram and velocity vectors for a higher density peak halo are shown in Fig. 19. The masses of the minihaloes in this case are 9×10^5, 6×10^5, 5×10^5, 3×10^5, 2.6×10^4 and $9 \times 10^4\,M_\odot$. Stars are most likely to form in the H_2-cooled minihaloes. The sizes of the clumps are bigger than the H_2-cooled fragments due to a difference in the Jeans masses. Fragmentation to lower than the Jeans scale is not possible as gas becomes pressure supported.

We also see that the entropy of the gas is increased up to 0.1 keV cm^2 by trapping Lyman α photons. It is increased in shocks and lost due to cooling. Complete entropy calculations are beyond the scope of this paper. We have not included the feedback effects from the first objects in our simulations. The presence of UV flux from Population III stars will suppress the formation of H_2 (Dijkstra & Loeb 2009; Shang et al. 2010). Further fragmentation will be inhibited in these haloes. It will support the mode of the formation of massive objects in the haloes that we consider here. It should be noted in this that star formation is not completely

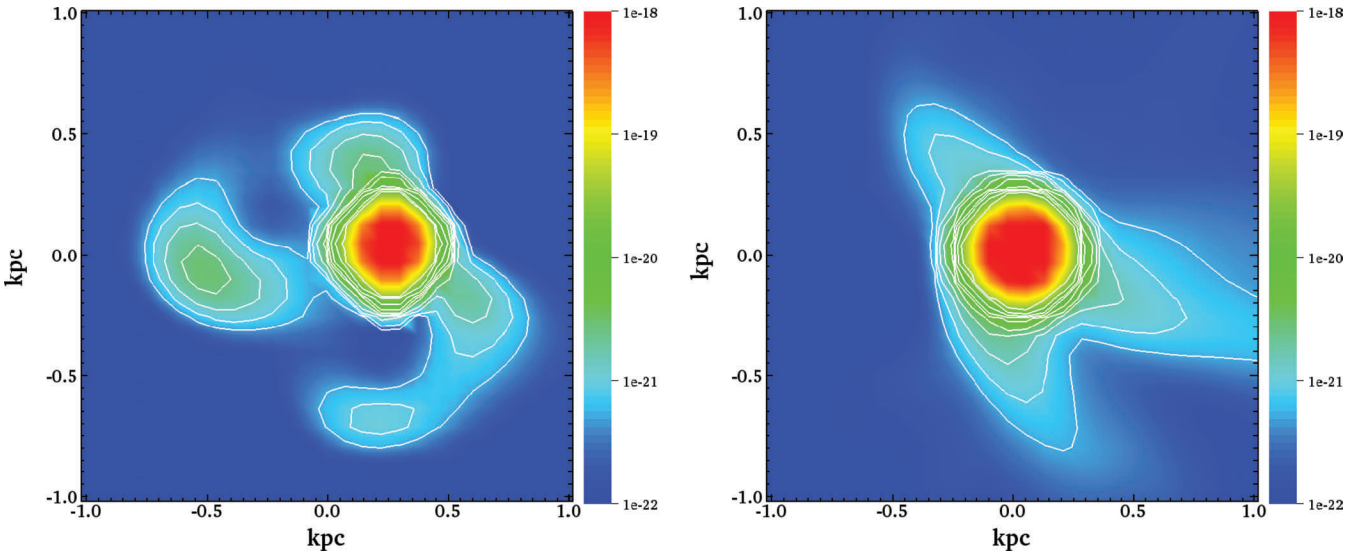

Figure 17. Density slices of the inner 2-kpc region (zoomed) of Figs 16 (left-hand panel) and 15 (right-left panel). The left-hand panel shows the density slice for the atomic cooling case. The right-hand panel shows the density slice for the Lyman α case. Contours are overplotted to show the density structure. Distance scales are in comoving units. Here, 1 kpc in comoving units corresponds to 53 pc in proper units.

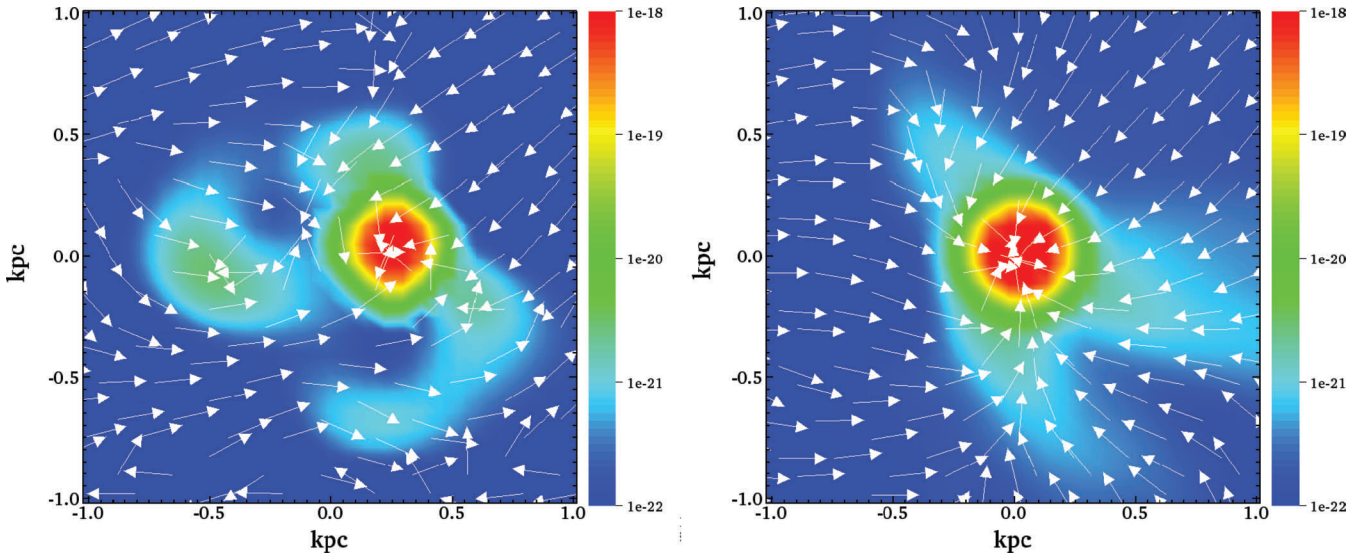

Figure 18. Velocity field corresponding to Fig. 17. The left-hand panel shows the velocity field for the atomic cooling case. The right-hand panel shows the velocity field for the Lyman α case. Velocity vectors represent the flow of gas after subtracting the background flow.

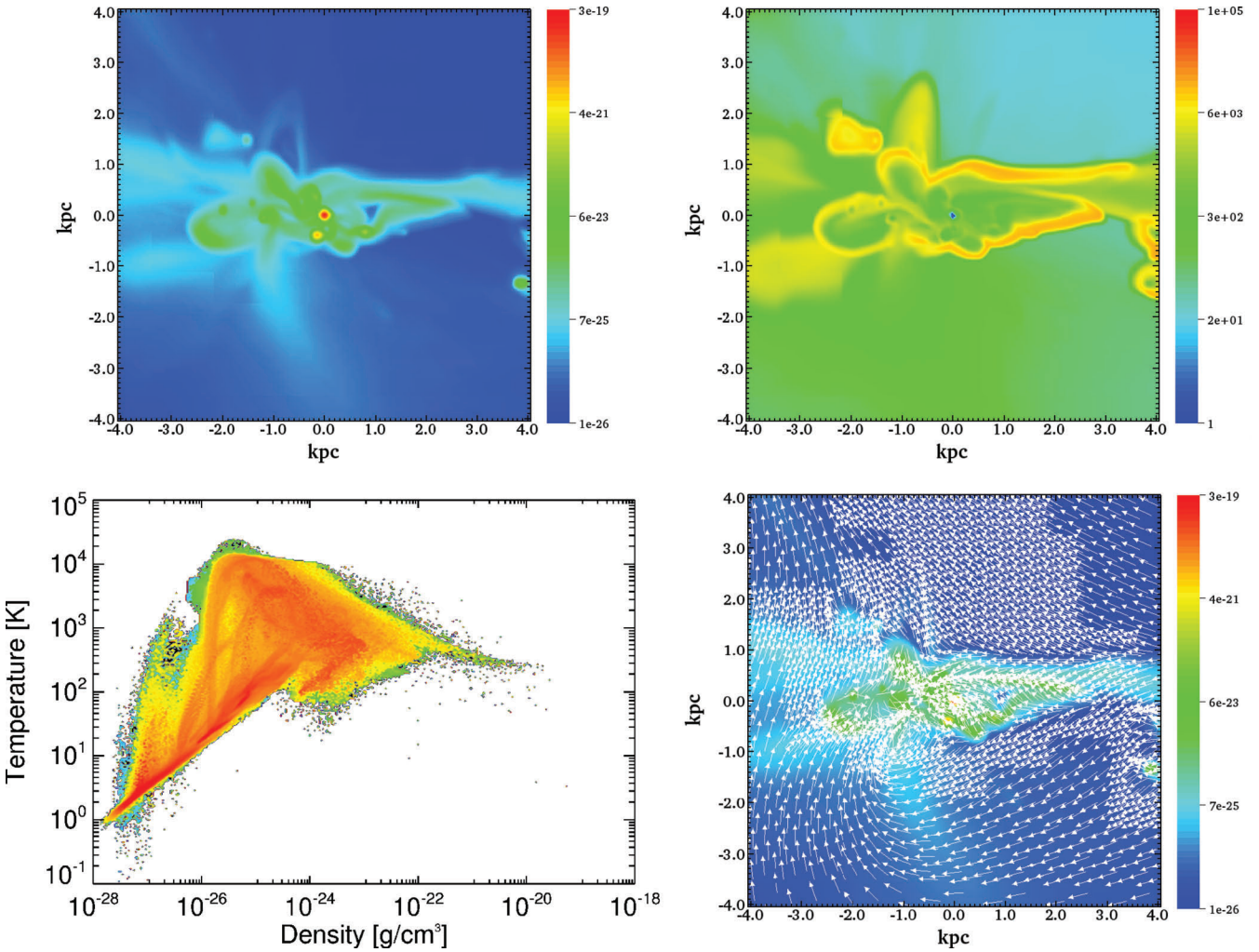

Figure 19. A higher density peak halo for the molecular hydrogen cooling case. The top-left panel shows the density slice through the centre of a halo. The temperature slice corresponding to the density slice is depicted in the top-right panel. The bottom-left panel shows the phase diagram. The flow of gas is seen in the bottom-right panel. Values corresponding to colours are shown in colour bars. Distance scales are in comoving units. Here, 1 kpc in comoving units corresponds to 53 pc in proper units.

suppressed by a UV background due to efficient self-shielding or positive feedback that results from shocks (Ricotti, Gnedin & Shull 2002; Johnson, Greif & Bromm 2007). X-rays from miniquasars can stimulate the formation of molecular hydrogen (Haiman et al. 2000). High columns present in our case will partly self-shield the gas from the feedback of X-rays, but the gas in the surrounding might be effected. Removal or redistribution of angular momentum is an obstacle in the formation of massive objects. The gas can transfer angular momentum via shock waves and bar instabilities (Wise et al. 2008; Larson 2010). We noted that gas becomes turbulent during virialization and helps in the dissipation of angular momentum. We do see strong shock waves occurring at low densities in our simulations which also play an important role in the distribution of angular momentum. Numerical simulations should be performed to get detailed insight into the angular momentum issue.

In any case, thermodynamical properties of the gas play an indispensable role in the fragmentation of gas cloud and the formation of primordial objects. Our results include radiative transfer effects of the Lyman α photons in an approximate manner, but still give good insight into radiative transfer effects on primordial gas physics. Forthcoming telescopes such as Low Frequency Array (LOFAR) and *James Webb Space Telescope* (JWST) will be able to observe the objects formed in the early Universe and will help to scrutinize the present paradigm of the formation of primordial objects.

ACKNOWLEDGMENTS

The FLASH code was in part developed by the DOE-supported Alliance Center for Astrophysical Thermonuclear Flashes (ACS) at the University of Chicago. Our simulations were carried out on the Gemini machines at the Kapteyn Astronomical Institute, University of Groningen. We would like to pay special thanks to Seyit Hocuk for valuable discussions. We thank the anonymous referee for careful insight and useful comments.

REFERENCES

Abel T., Bryan G. L., Norman M. L., 2000, ApJ, 540, 39
Abel T., Bryan G. L., Norman M. L., 2002, Sci, 295, 93
Begelman M., Shlosman I., 2009, ApJ, 702, L5
Begelman M. C., Volonteri M., Rees M. J., 2006, MNRAS, 370, 289
Bertschinger E., 1995, preprint (astro-ph/9506070)
Borgani S., Finoguenov A., Kay S. T., Ponman T. J., Springel V., Tozzi P., Voit G. M., 2005, MNRAS, 361, 233
Bromm V., 2004, PASP, 116, 103
Bromm V., Larson R. B., 2004, ARA&A, 42, 79
Bromm V., Loeb A., 2003, ApJ, 596, 34
Bromm V., Loeb A., 2004, New Astron., 9, 353
Bromm V., Yoshida N., Hernquist L., McKee C. F., 2009, Nat, 459, 49
Childs H., Brugger E. S., Bonnell K. S., Meredith J. S., Miller M., Whitlock B. J., Max N., 2005, Proc. IEEE Visualization, A Contract-Based System for Large Data Visualization. p. 190, http://doi.ieeecomputersociety.org/10.1109/VIS.2005.3
Ciardi B., Ferrara A., 2005, Space Sci. Rev., 116, 625
Clark P. C., Glover S. C. O., Klessen R. S., Bromm V., 2010, preprint (arXiv:1006.1508)
Colella P., Woodward P. R., 1984, J. Computat. Phys., 54, 174
Dekel A. et al., 2009, Nat, 457, 451
Devecchi B., Volonteri M., 2009, ApJ, 694, 302
Dijkstra M., Loeb A., 2009, MNRAS, 400, 1109
Dijkstra M., Haiman Z., Mesinger A., Wyithe J. S. B., 2008, MNRAS, 391, 1961
Djorgovski S. G., Volonteri M., Springel V., Bromm V., Meylan G., 2008, preprint (arXiv:0803.2862)
Fardal M. A., Katz N., Gardner J. P., Hernquist L., Weinberg D. H., Davé R., 2001, ApJ, 562, 605
Fryxell B. et al., 2000, ApJS, 131, 273
Galli D., Palla F., 1998, A&A, 335, 403
Greif T. H., Johnson J. L., Klessen R. S., Bromm V., 2008, MNRAS, 387, 1021
Greif T. H., Glover S. C. O., Bromm V., Klessen R. S., 2010, ApJ, 716, 510
Haiman Z., 2004a, ApJ, 613, 36
Haiman Z., 2004b, KITP Conf., Galaxy-Intergalactic Medium Interactions Formation of the Earliest Stars and Black Holes and their Contribution to Reionization, http://online.kitp.ucsb.edu/igm_c04/haiman
Haiman Z., Spaans M., 1999, ApJ, 518, 138
Haiman Z., Abel T., Rees M. J., 2000, ApJ, 534, 11
Hui L., Gnedin N. Y., 1997, MNRAS, 292, 27
Johnson J. L., Greif T. H., Bromm V., 2007, ApJ, 665, 85
Johnson J. L., Greif T. H., Bromm V., 2008, MNRAS, 388, 26
Kereš D., Katz N., Fardal M., Davé R., Weinberg D. H., 2009, MNRAS, 395, 160
Larson R. B., 2010, Rep. Progress Phys., 73, 014901
Li Y., Klessen R. S., Mac Low M., 2003, ApJ, 592, 975
McKee C. F., Tan J. C., 2008, ApJ, 681, 771
Neufeld D. A., 1991, ApJ, 370, L85
Oh S. P., Haiman Z., 2002, ApJ, 569, 558
Omukai K., Schneider R., Haiman Z., 2008, ApJ, 686, 801
O'Shea B. W., Norman M. L., 2007, ApJ, 654, 66
Palla F., Salpeter E. E., Stahler S. W., 1983, ApJ, 271, 632
Peebles P. J. E., Dicke R. H., 1968, ApJ, 154, 891
Portegies Zwart S. F., Baumgardt H., Hut P., Makino J., McMillan S. L. W., 2004, Nat, 428, 724
Rees M. J., 1978, Observatory, 98, 210
Rees M. J., Ostriker J. P., 1977, MNRAS, 179, 541
Regan J. A., Haehnelt M. G., 2009a, MNRAS, 393, 858
Regan J. A., Haehnelt M. G., 2009b, MNRAS, 396, 343
Ricker P. M., 2008, ApJS, 176, 293
Ricotti M., Gnedin N. Y., Shull J. M., 2002, ApJ, 575, 49
Scalo J., Biswas A., 2002, MNRAS, 332, 769
Schleicher D. R. G., Spaans M., Glover S. C. O., 2010, ApJ, 712, L69
Shang C., Bryan G. L., Haiman Z., 2010, MNRAS, 402, 1249
Spaans M., Silk J., 2000, ApJ, 538, 115
Spaans M., Silk J., 2006, ApJ, 652, 902
Springel V., Hernquist L., 2002, MNRAS, 333, 649
Sutherland R. S., Dopita M. A., 1993, ApJS, 88, 253
Tegmark M., Silk J., Rees M. J., Blanchard A., Abel T., Palla F., 1997, ApJ, 474, 1
Trenti M., Stiavelli M., Michael Shull J., 2009, ApJ, 700, 1672
Truelove J. K., Klein R. I., McKee C. F., Holliman II J. H., Howell L. H., Greenough J. A., 1997, ApJ, 489, L179
Wise J. H., Abel T., 2007, ApJ, 665, 899
Wise J. H., Turk M. J., Abel T., 2008, ApJ, 682, 745
Yoshida N., Omukai K., Hernquist L., Abel T., 2006, ApJ, 652, 6

This paper has been typeset from a TEX/LATEX file prepared by the author.